Biosensors and Bioelectronics 126 (2019) 758–766

Contents lists available at ScienceDirect

Biosensors and Bioelectronics

journal homepage: www.elsevier.com/locate/bios

Simultaneous detection of ATP metabolites in human plasma and urine based on palladium nanoparticle and poly(bromocresol green) composite sensor

Mamta Raj[a], Jong-Min Moon[b], Rajendra N. Goyal[a,*], Deog-Su Park[c], Yoon-Bo Shim[b,*]

[a] Department of Chemistry, Indian Institute of Technology Roorkee, Roorkee 247667, India
[b] Department of Chemistry and Institute of BioPhysio Sensor Technology (IBST), Pusan National University, Busan 46241, Republic of Korea
[c] Institute of BioPhysio Sensor Technology (IBST), Pusan National University, Busan 46241, Republic of Korea

ARTICLE INFO

Keywords:
Electrochemical sensor
Adenosine triphosphate metabolites
Palladium nanoparticles
Poly-bromocresol green
Functionalized carbon nanotubes

ABSTRACT

A sensitive voltammetric sensor based on palladium nanoparticles (PdNPs) and poly-bromocresol green (pBG) composite layer immobilized on amide functionalized single-walled carbon nanotubes (AmSWCNTs) modified pyrolytic graphite (PdNPs:pBG/AmSWCNTs/PG) has been prepared for the simultaneous determination of adenosine triphosphate (ATP) catabolites, inosine (INO), hypoxanthine (HX), xanthine (XT), and uric acid (UA). The modified PdNPs:pBG/AmSWCNTs/PG was characterized by electrochemical experiments and surface analysis, which exhibited exceptional electrocatalytic effects towards the oxidation of INO, HX, XT, and UA with a significant enhanced peak current and well resolved peaks separation for all the analytes. The linear calibration curves were obtained in the concentration range of 0.001–175 μM, 0.001–200 μM, 0.001–150 μM, and 0.001–200 μM and limits of detection were found as 0.95 nM, 1.04 nM, 1.07 nM, and 0.43 nM corresponding to INO, HX, XT, and UA, respectively. The common metabolites present in the biological fluids did not interfere in the determination. The applicability of the proposed sensor was successfully demonstrated by determining INO, HX, XT, and UA in the human plasma and urine and the obtained results were validated by using HPLC.

1. Introduction

Adenosine triphosphate (ATP) is used in cells as a coenzyme and transports chemical energy with in cells for metabolism. In the human system, metabolism of ATP occurs by a series of enzymatic reactions (Scheme 1). Initially the breakdown leads to cellular accumulation of adenosine diphosphate (ADP) and adenosine monophosphate (AMP) and activates some dormant enzymes including AMP deaminase, 5′-nucleotidase, xanthine oxidase, and purine nucleoside phosphorylase. In this case, inosine (INO) can be produced by two different pathways. In one way, AMP deaminase catabolizes AMP into inosine monophosphate (IMP), which is converted by the 5′-nucleotidase to INO. Otherwise, AMP is cleaved by either intra- or extra-cellular 5′-nucleotidase to form adenosine, which is subsequently converted to INO by adenosine deaminase (Hasko et al., 2004; Hussain et al., 2018). INO is then converted into hypoxanthine (HX) and finally xanthine oxidase converts HX to xanthine (XT) and subsequently to uric acid (UA) (Farthing et al., 2015; Pedley and Benkovic, 2017; Amorini et al., 2009). INO, the major metabolite of ATP degradation performs various important functions in the human body, such as, participation in tumor necrosis factor, which induces nitric oxide production in cultured sertoli cells, protection against myocardial damage, participation in receptor mediated signaling, having inflammatory and immune modulatory effects, reduction of LPS-induced acute lung injury and association with multiple sclerosis (Souza et al., 2005; Liaudet et al., 2001; Buckley et al., 2005; Revin and John, 2012). INO is found in the micro molar range (0.75–1.49 μM) in interstitial fluids, whereas the level increases fiercely during ischemia and sepsis interstitial and reaches greater than 1.0 mM (Welihinda et al., 2016). HX, is found in low concentration as 1.47–2.94 μM in blood plasma and is also a potential biomarker for acute cardiac ischemia (AMI), where the concentration of HX elevated in the bloodstream (Farthing et al., 2015; Camba et al., 2014). Further conversion of HX to XT, which is found in the physiological fluids as 20 μg/dL is important to measure as the level of xanthine is required for the diagnosis and treatment of Gouty arthritis (gout), hyperuricaemia, and xanthinuria (Bas et al., 2011). The final metabolic product UA is produced in liver, intestines and other tissues and is normally excreted via urine. The release of ATP-

* Corresponding authors.
E-mail addresses: rngcyfcy@gmail.com, rngcyfcy@iitr.ac.in (R.N. Goyal), ybshim@pusan.ac.kr (Y.-B. Shim).

https://doi.org/10.1016/j.bios.2018.11.056
Received 11 October 2018; Received in revised form 14 November 2018; Accepted 24 November 2018
Available online 08 December 2018
0956-5663/

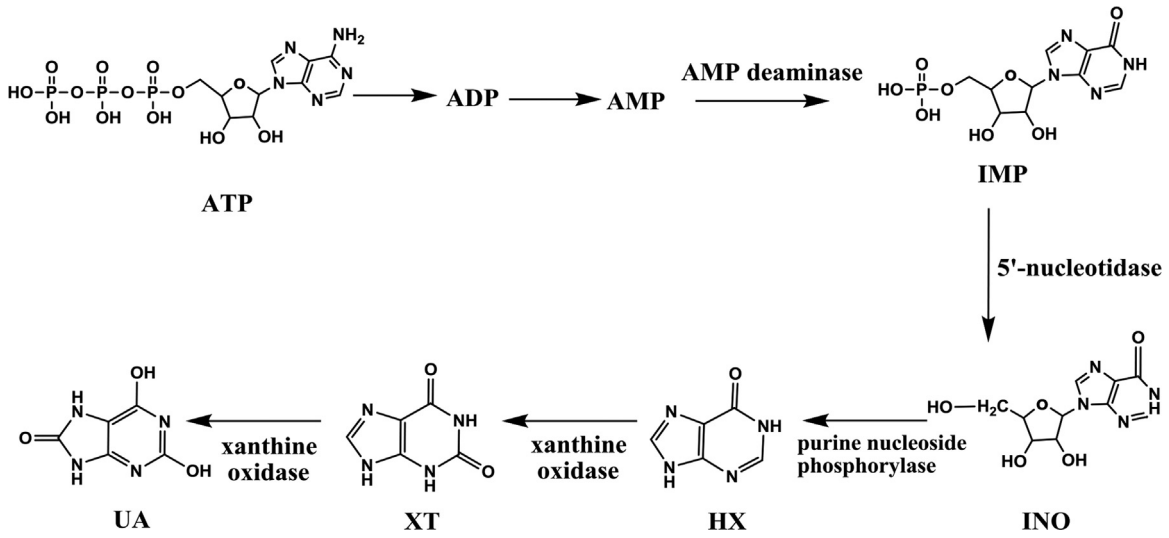

Scheme 1. A series of enzymatic reactions that occur during ATP catabolism.

catabolites was less in newborn than in the adults' hearts during reperfusion, which coincided with lower xanthine oxidase activity (Farthing et al., 2015). In the patients with AMI, angina pectoris and other ischemic diseases, a significant rise in the intermediates and end products of purine metabolism i.e. INO, HX, XT, and UA can be an indicator of a heart attack (Augusto et al., 2014). Hence, the simultaneous determination of these four ATP catabolites has been considered of significant importance in biochemical and clinical diagnosis.

The determinations of INO, HX, XT, and UA were carried out by several methods, such as high-performance liquid chromatography, reverse-phase chromatography, chemiluminescent, liquid chromatography with a diode array detector, capillary electrophoresis, spectrophotometer, multi-enzyme reactor sensor and many more (Cooper et al., 2006; Farthing et al., 2007, 2011; Maiuolo et al., 2016; Hamzah et al., 2013; Richter et al., 2002; Okuma and Watanabe, 2002; Wang et al., 2009). An enzyme-coupled assay for fluorometric detection of AMP, adenosine, INO, and HX, was reported, however, the procedure required costly apparatus, complicated enzyme reactions, and extensive analysis time (Helenius et al., 2012). To our knowledge, no attempt has been made to determine these four metabolites simultaneously without any separation technique in the last decade. However, most of the reported methods used for the individual and simultaneous determination of two purines have many limitations, like less sensitivity, long analysis time and poor selectivity, involvement of complex steps for sample preparation and requirement of expensive instruments. Therefore a rapid, less expensive, highly sensitive and selective technique is required for the simultaneous determination of these four metabolites. In the presented approach, amide functionalized SWCNTs (AmSWCNTs) were combined with the film of palladium nanoparticles (PdNPs) and polymer of bromocresol green (pBG) for enhancing the macroscopic mechanical properties of the composite. Amide functionalized SWCNTs were used to improve the nanotube-polymer interface as the amine termination of the nanotubes provides the suitable link for covalent bonding via amide linkage between SWCNTs and biological molecules or pBG layer (Ramanathan et al., 2005; Kim et al., 2013). PdNPs are used as a surface modifier due to the compatibility with biomolecules (Atta and Kady, 2010; Rastogi et al., 2014). In the present method, first AmSWCNTs was casted at the pyrolytic graphite surface followed by electro polymerization of BG in the presence of $PdCl_2$. The modified probe layers were characterized by field emission scanning electron microscopy, high resolution transmission electron microscopy, X-ray photoelectron spectroscopy, electrochemical impedance spectroscopy, cyclic voltammetry, and square wave voltammetry. The modification exhibited excellent electrocatalytic activity, larger effective surface area, good conductivity, improved biocompatibility and helped in the sensitive simultaneous determination of INO, HX, XT, and UA.

2. Experimental

2.1. Materials and chemicals

INO, HX, XT, UA, SWCNTs (code 519308 Sigma), BG, and ethylenediamine and *N*-[(dimethylamino)-1*H*-1,2,3-triazolo[4,5,6]pyridin-1-ylmethylene]-*N*-methylmethanaminium hexafluorophosphate *N*-oxide (HATU) were purchased from Sigma-Aldrich (USA). The pieces of pyrolytic graphite ($10 \times 3 \times 3\,mm^3$) were received from Pfizer Inc. New York, USA as a gift. The phosphate buffers in the pH range 2.4–10.5 ($\mu = 1.0$ M) were prepared by reported method (Christian and Purdy, 1962). Considering the physiological pH, the phosphate buffer of pH 7.4 was used for detailed experimental studies.

2.2. Instruments

The voltammetric measurements were performed in a three-electrode electrochemical cell consisting of a pyrolytic graphite working, a platinum electrode as the counter, and Ag/AgCl (3 M NaCl) as the reference electrode using bio-analytical system (BAS, West Lafayette, USA) Epsilon EC-USB workstation. The morphological characterization of the modified surface has been carried out using Field Emission Scanning Electron Microscopy (FE-SEM, Zeiss ultra plus 55), High resolution transmission electron microscopy (HR-TEM, JEOL, JEM-300FS), and Fourier-transform infrared spectroscopy (FTIR, PerkinElmer, Inc-L1600300 Spectrum Two LITs/96903). The X-ray photoelectron spectroscopy (XPS) was analyzed using VG Scientific XPSLAB 250 XPS spectrometer and a monochromated Al Kα source with charge compensation (KBSI (Busan)). The electrochemical impedance spectroscopic studies (EIS) were carried out by using a Versastat 3 (PAR, USA) to determine the charge transfer resistance of the fabricated surface.

2.3. Preparation of amide functionalized SWCNTs

The amide functionalization of SWCNTs involved two steps (Ramanathan et al., 2005; Ciobotaru et al., 2013). In the first step, SWCNTs (20 mg) were treated with a 3:1 mixture of conc. H_2SO_4 and HNO_3 solution (30 ml) and reaction mixture was sonicated in an ultrasonic bath at 40 °C for 3 h to introduce carboxylic acid (-COOH) groups on the surface of SWCNTs. After 3 h, the reaction mixture was

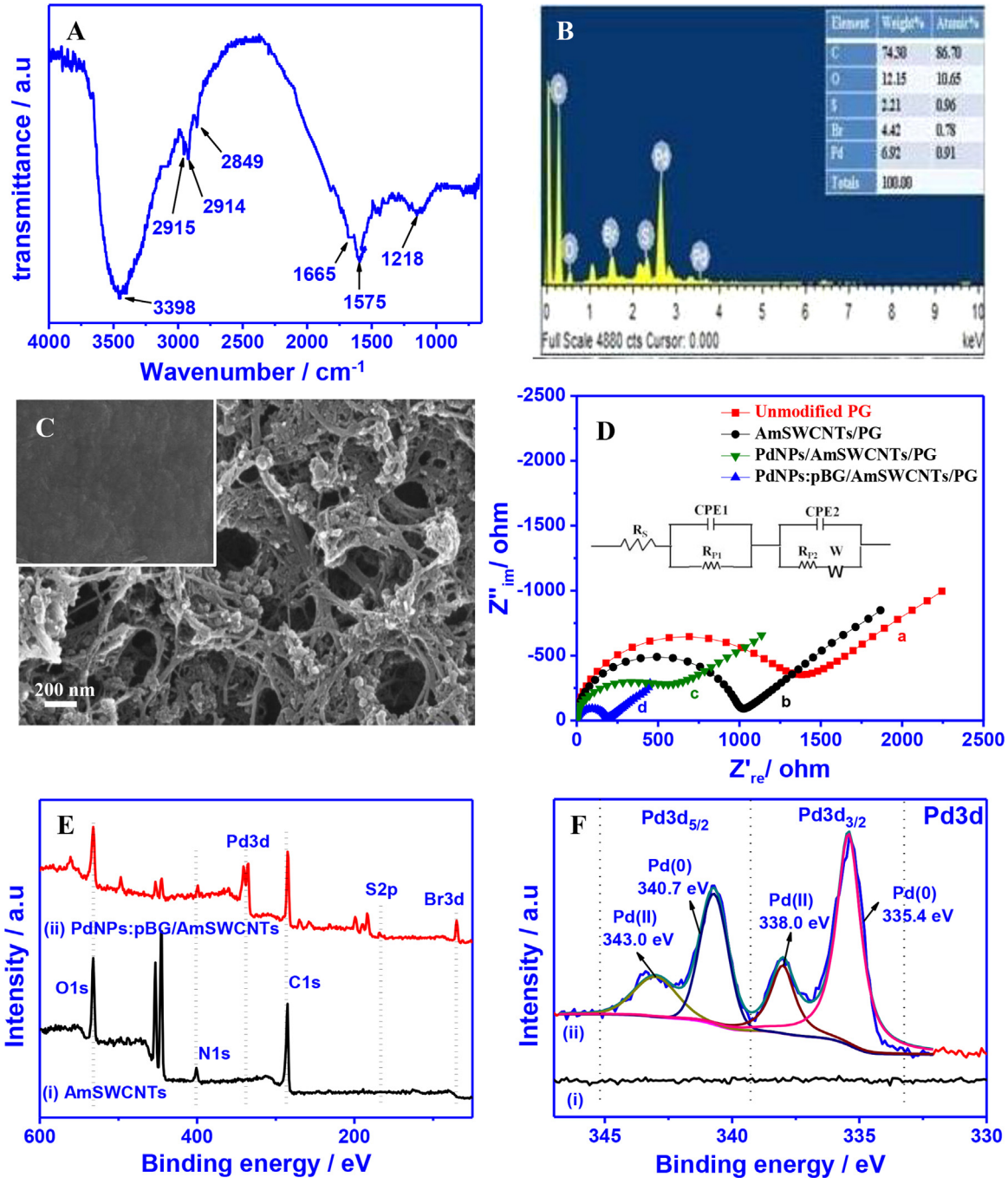

Fig. 1. FT-IR spectrum observed for amide-functionalized SWCNTs (A), EDX data demonstrating the presence of Pd in PdNPs:pBG/AmSWCNTs/PG (B). Typical FE-SEM images observed for PdNPs:pBG/AmSWCNTs/PG and inset shows the unmodified PG (C). Typical Nyquist plots observed for unmodified PG (a), AmSWCNTs/PG (b), PdNPs/AmSWCNTs/PG (c), and PdNPs:pBG/AmSWCNTs/PG (d). The inset shows the Randle's equivalent circuit used for the simulation of the EIS data. XPS survey spectra of (i) AmSWCNTs and (ii) PdNPs:pBG/AmSWCNTs (E) and Pd3d (F).

added drop-wise to the cold double distilled water and then filtered using polycarbonate filter paper (10 μm pore size). The residual acid was then removed by washing with double distilled water and the residue was dried at 80 °C for 4 h. In the next step, the oxidized SWCNTs (15 mg) were added in 10 ml of ethylenediamine and the mixture was sonicated. The coupling agent HATU (1 mg) was then added to the reaction mixture and sonicated for 4 h. The methanol in excess amount was then added to the mixture and product was filtered using polycarbonate filter paper. The residue was washed with excess of methanol. The prepared amide functionalized SWCNTs (AmSWCNTs) were dried at 80 °C for ~24 h.

2.4. Preparation of polymer nanocomposite modified PdNPs: pBG/AmSWCNTs/PG

An unmodified PG sensor was prepared by reported method (Goyal et al., 1985). The optimized volume of 10 μL of prepared AmSWCNTs (1 mg/ml dispersed in dimethylformamide solution was drop-casted at the surface of sensor and allowed to dry overnight in an oven at 110 °C (S.I. – 1). DMF is selected as it is suitable solvent for the dispersion of various functionalized nanotubes because it properly wets the nanotubes (Vaisman et al., 2006). In the next step, 1:1 mixture of 1 mM $PdCl_2$ (prepared in 10% HCl) and 1.0 mM BG (prepared in 0.1 M NaOH)

were taken and the AmSWCNTs deposited PG sensor was dipped in it and potential was applied from -400–1800 mV at a sweep rate of 100 mV/s for 20 scans (optimized, S.I. – 1). On completion of 20 scans the resulting surface was thoroughly washed with double distilled water to remove unreacted molecules at the surface of sensor. The modified surface was characterized using FE-SEM and HR-TEM. For recording voltammograms the prepared PdNPs: pBG/AmSWCNTs/PG sensor was first stabilized by scanning the potential from 400 mV to −1100 mV for 5 cycles at 100 mV/s sweep rate in 0.1 M NaOH solution to get a steady cyclic voltammogram because pBG gets deprotonation at higher pH to give the dianionic form, which is stabilized by resonance structure (Shokrollahi and Firoozbakht, 2016) as shown in S.I. Fig. 1. In another approach, electro-deposition of PdNPs: pBG composite (by scanning the potential from 400 mV to −1100 mV for 5 cycles at 100 mV/s sweep rate) was first achieved, followed by the drop casting of AmSWCNTs. In this case, broad anodic peaks with low currents and higher potential were observed for the analytes. Hence, electro-deposition of PdNPs: pBG was carried out after drop-casting of AmSWCNTs at the PG surface (first approach) to ensure good conductivity and sensitivity, which was used for further studies.

2.5. Experimental procedure

For the voltammetric studies, 1.0 mM solutions of four analytes INO, HX, XT and UA were prepared in double distilled water. Then 2.0 ml of phosphate buffer (pH 7.4), desired amount of analyte and remaining water (total 4 ml) were used. The optimized parameters used in cyclic voltammetry were initial potential (Ei): 0 mV, switching potential (E): 1500 mV, final potential (Ef): 0 mV, sweep rate (v): 100 mV/s. The parameters used in square wave voltammetry (SWV) were Ei: 0 mV, Ef: 1500 mV, square wave frequency (f): 15 Hz, square wave amplituse (Esw): 25 mV and potential step (E): 4 mV. To remove the adsorbed material and regenerate the sensing surface at constant potential of −800 mV was applied in the blank solution for 180 s after each scan. The potentials reported are with respect to Ag/AgCl electrode.

To ensure the practical applicability of the modified sensor human urine and blood plasma sample of healthy volunteers were obtained from Indian Institue of Technology (I.I.T.), Roorkee hospital (approved by Institutional Human Ethics Committee (IHEC), No: BIOTECH/IHEC/AP/15/1). The collected urine and plasma samples were diluted two times with phosphate buffer of pH 7.4 prior to analysis to minimize matrix complexity. For the validation of results obtained, HPLC was carried out by using Shimadzu LC-2010A HT system equipped with C_{18} bondapack 125 Å, 10 μm) reverse phase column. The mobile phase used was 50 mM phosphate buffer (48 mM of KH_2PO_4 and 2 mM K_2HPO_4 with methanol (97:3, v/v) followed by adjusting the pH to 4.0) at the flow rate of 0.5 ml/min. The injection volume of the sample was 40 μL and the absorbance of the eluent was monitored at 285 nm.

3. Results and discussion

3.1. Characterization of sensor

The prepared AmSWCNTs were characterized by recording FT-IR spectra and the observed results are displayed in Fig. 1A, in which a band at 1665 cm^{-1} corresponding to the amide carbonyl (C=O) stretching was noticed. Two other bands at 1575 cm^{-1} and 1218 cm^{-1} are assigned to the N-H in-plane and C-N bond stretching, respectively and further confirmed the presence of the amide functional group. A broad band at 3398 cm^{-1} is due to the characteristic N-H stretching vibrations and C-H stretches are observed between 2849 cm^{-1} and 2915 cm^{-1}. The observed results are similar to the previously reported in the literature for amide functionalized SWCNTs (Chidawanyika and Nyokong, 2010; Ramanathan et al., 2005). To demonstrate the presence of Pd at the surface, EDX was performed at the modified surface (Fig. 1B), which clearly indicated the presence of Pd in PdNPs: pBG/AmSWCNTs/PG sensor.

Surface morphology of the modified sensor was carried out by using FE-SEM. Some typical images observed are presented in Fig. 1C. The surface of the unmodified PG surface is smooth and flat as represented in the inset of Fig. 1C. The surface of PdNPs: pBG/AmSWCNTs/PG sensor had herbs like clusters appeared to be interlinked with amino groups and provided increased nanotubes/metal nanoparticle-polymer interface, which facilitate the interaction and electron transfer property between the analyte and modified surface. S.I. Fig. 2 shows the (A, B) HR-TEM images of PdNPs: pBG layer and (C) corresponding EDX analysis result, which can clearly see the small PdNPs (average size of 5 nm) were formed on the pBG layer with well distribution and high density. Additionally, evidence for the presence of PdNPs in the pBG layer was obtained by EDX analysis.

EIS was used to investigate the electrochemical characteristics of the sensor at different stages of modification. The values of the electron-transfer resistance (R_{CT}) were determined in 0.1 M KCl containing 2.0 mM $K_3Fe(CN)_6$ solutions over a frequency range of 0.1–100 Hz with an applied potential of 50 mV. The EIS curves displayed a semicircle followed by the linear portion (Fig. 1D) in which the semicircular portion featured an electron transfer limiting process, whereas the charge transfer resistance (R_{CT}) was equal to the diameter of the semicircle. The inset of the (Fig. 1D) shows the Randle's equivalent circuit used for simulating the experimental data, where Rs denotes the electrolyte resistance; double layer capacitance (CPE) denotes the double layer capacitance and W stand for Warburg impedance. Unmodified PG surface exhibited a large semicircle portion indicating high R_{CT} (1198 Ω) for the $Fe(CN)_6^{3-/4-}$ redox process (curve a), whereas the charge transfer rate at electrode/electrolyte surface was higher for modified electrode, hence, the impendence would decrease due to the conductivity of SWCNTs and high electrochemical activity due to amide functionalization (Wang et al., 2016). Thus, AmSWCNTs/PG exhibited a reduced semicircular domain with the R_{CT} value as 986 Ω (curve b). The observed R_{CT} value for PdNPs/AmSWCNTs/PG is 563 Ω (curve c) and in the case of PdNPs: pBG/AmSWCNTs/PG sensor, the smallest semicircle was witnessed with the R_{CT} value as 188 Ω (curve d) indicating lowest resistance for this sensor. Thus, it is concluded that PdNPs: pBG/AmSWCNTs/PG sensor has lowest resistance and maximum electron transfer efficiency, which would promote the oxidation of ATP metabolites.

Fig. 1E-F and S.I. Fig. 3 shows the XPS analysis using (i) AmSWCNTs and (ii) PdNPs: pBG/AmSWCNTs modified layer with survey (Fig. 1E), Pd3d (Fig. 1F), C1s (S.I. Fig. 3A), S2p (S.I. Fig. 3B), and Br3d (S.I. Fig. 3C). All spectra were internally calibrated with the C1s peak (284.6 ev) before analysis. The deconvoluted C1s spectrum revealed three peaks at 284.6, 285.9, and 288.5 eV, which corresponded to the C-C or C=C, C-N, and C-O or C=O bonds, respectively. The C-N peak was observed, which indicated the presence of C-N bond from the amide functionalized SWCNTs. Moreover, the C-O or C=O peak appeared because of SWCNTs, that comprises abundant of carboxylic acid or carbonyl groups. In addition, S2p (C-S (163.1 eV) and S-O or S=O (168.0 eV)) and Br3d (Br-C (70.2 eV)) peaks were newly obtained for the PdNPs: pBG/AmSWCNTs modified layer, and were originated from pBG. Moreover, XPS spectrum of Pd3d was characterized by two spin-orbit-split doublets ($3d_{5/2}$ and $3d_{3/2}$). The major two peaks at 335.4 and 340.7 eV indicates the bulk metallic Pd (Pd(0)), however, relatively small peaks at 338.0 and 343.0 eV are attributed from the chemically bound Pd (Pd(II)). From the result of S2p, Br3d, and Pd3d spectra, we have confirmed that the PdNPs: pBG layer was successfully immobilized on the AmSWCNTs, while no peaks were observed at S2p, Br3d, and Pd3d for the AmSWCNTs layer due to the absence of each atom.

3.2. Cyclic voltammetry

Cyclic voltammograms were recorded in 1.0 mM $K_3Fe(CN)_6$ containing 0.1 M KCl at different sweep rates (5 mV/s to 225 mV/s). The

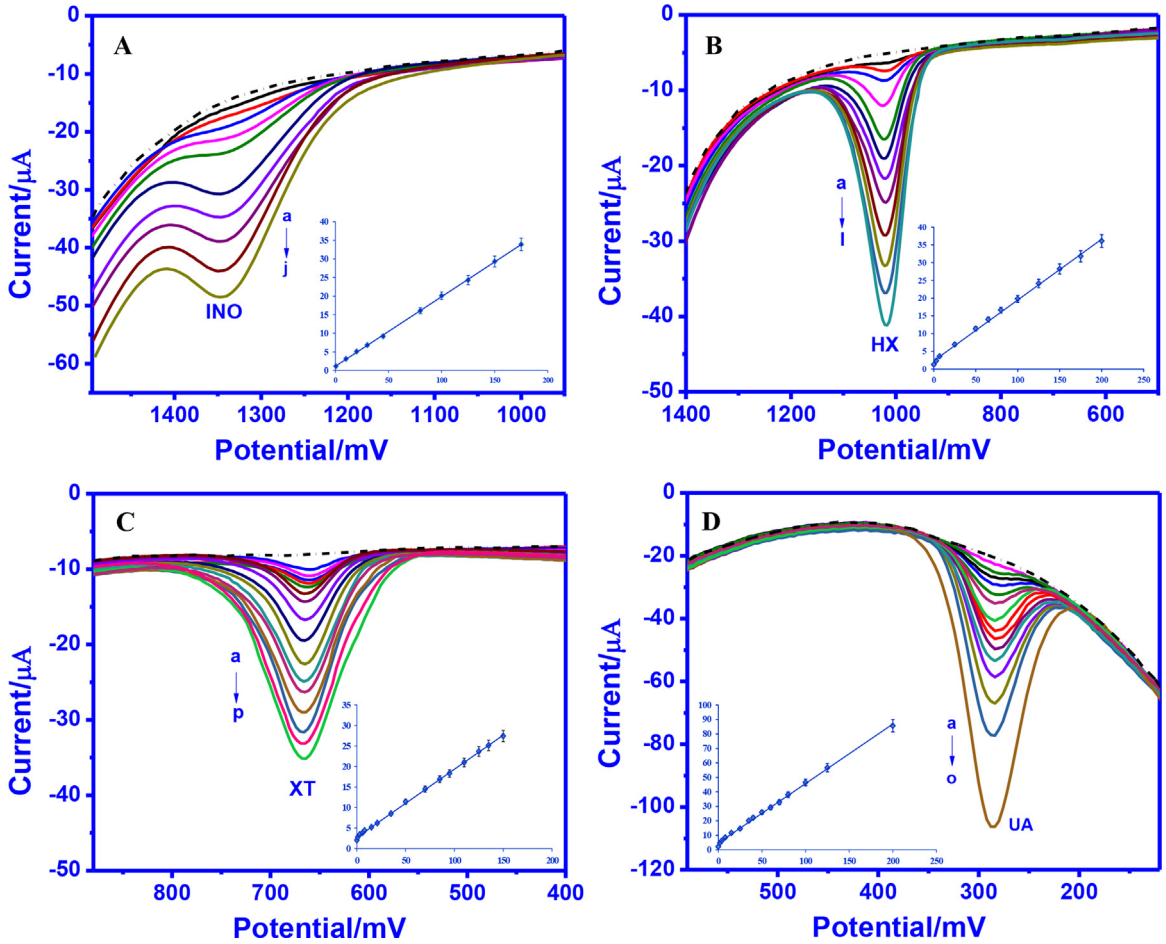

Fig. 2. SWVs observed for the increasing concentration of (A) INO (0.001 − 200 μM), (B) HX (0.001 − 200 μM), (C) XT (0.001 − 150 μM), and (D) UA (0.001 − 200 μM) at PdNPs:pBG/AmSWCNTs/PG sensor. Each inset figure shows the corresponding calibration plot.

observed slope of the ip vs. $\nu^{1/2}$ plots was used to calculate effective surface areas using Randles-Sevcik equation. The calculated value of effective surface areas for unmodified PG, AmSWCNTs/PG, PdNPs/AmSWCNTs/PG, and PdNPs: pBG/AmSWCNTs/PG were found as 0.086 cm^2, 1.732 cm^2, 2.988 cm^2, and 3.894 cm^2, respectively. The highest effective surface area was found for the PdNPs: pBG/AmSWCNTs/PG sensor, which was nearly 45 times greater than unmodified PG and increased the charge transfer kinetics for the electro-oxidation of the targeted analytes.

The voltammograms of a mixture of these analytes were recorded having INO, HX, and XT (25 μM), and UA (10 μM) at unmodified PG, AmSWCNTs/PG and PdNPs: pBG/AmSWCNTs/PG as shown in the (S.I. Fig. 4A). At unmodified PG surface, three anodic peaks were observed. The broad peak at 1110 mV was due to INO and HX (peak a_1) and other two peaks observed at 710 mV (peak a_2) and 307 mV (peak a_3) were due to XT and UA, respectively. Thus, unmodified PG surface was unable to separate the four analytes. At the surface of AmSWCNTs/PG sensor, four oxidation peak clearly observed with increased peak current and less peak potential at 1329 mV, 1057 mV, 690 mV, and 300 mV for INO (peak b_1), HX (peak b_2), XT (peak b_3), and UA (peak b_4), respectively, whereas at the surface of PdNPs/AmSWCNTs/PG sensor oxidation peaks were observed at 1320 mV, 1043 mV, 685 mV, and 290 mV for INO (peak c_1), HX (peak c_2), XT (peak c_3), and UA (peak c_4), respectively. At the surface of PdNPs: pBG/AmSWCNTs/PG sensor all the four peaks observed had large peak currents and peak potentials shifted to less positive potentials as 1342 mV (peak d_1), 1025 mV (peak d_2), 680 mV (peak d_3), and 293 mV (peak d_4) for INO, HX, XT, and UA, respectively.

The voltammograms were then recorded at the fixed concentration of 25 μM of each analyte in the sweep range 5 mV/s to 225 mV/s. It was observed that the peak current (ip) increased linearly with increasing sweep rate for all the analytes. The plots of ip versus ν and log ip versus log υ plots were linear and the relations and R^2 values are summarized (S.I. – 2). The linearity of ip versus υ plots suggested the involvement of adsorption controlled process for oxidation. Further, the slope of log ip versus log υ plots were 0.9407, 0.8335, 0.8529, and 0.8187 for INO, HX, XT and UA, respectively, which are sufficiently greater than 0.5 and confirmed adsorption controlled oxidation of these analytes (Zen et al., 2002; Raj et al., 2017).

3.3. Square wave voltammetry

Square wave voltammograms were recorded for a mixture of INO, HX, XT, and UA (25 μM each) at pH 7.4. A comparison of voltammograms at unmodified PG, AmSWCNTs/PG, PdNPs/AmSWCNTs/PG, and PdNPs: pBG/AmSWCNTs/PG sensors is shown in S.I. Fig. 4B. At unmodified PG (curve a) four peaks were obtained at 1358 mV, 1070 mV, 718 mV, and 296 mV for INO, HX, XT, and UA. At the AmSWCNTs/PG surface (curve b) and PdNPs/AmSWCNTs/PG surface (curve c) the peak potential shifted to more positive values in contrast to unmodified PG surface and enhanced peak currents were observed. However, PdNPs: pBG/AmSWCNTs/PG sensor surface (curve d) gives excellent results in terms of peak separation with the lowest peak potentials and sensitivity. The shift of Ep to less potential demonstrated the excellent electrocatalytic activity towards the simultaneous determination of these analytes due to the improvement in the interfacial binding, strength

and electron transfer properties.

3.3.1. Effect of pH

The effect of pH on the electrochemical behavior of different analytes was studied in the pH range 2.4–10.5 (μ = 0.1 M) at 25 μM concentration at the surface of PdNPs: pBG/AmSWCNTs/PG. The peak potential was dependent on pH and shifted towards less positive value with increasing pH. The Ep versus pH relation was linear (S.I. – 3). The value of d*Ep*/pH for all the analytes was close to 59 mV/pH (theoretical Nernst value), hence, it is concluded that equal number of electrons and protons are involved in the oxidation of these analytes at PdNPs: pBG/AmSWCNTs/PG sensor. The variation of peak current with pH for all the four metabolites is presented in S.I. Fig. 5.

The effect of square wave frequency on the oxidation peak current was studied over the frequency range 5–40 Hz at pH 7.4. An increase in the frequency induces an increase in the oxidation peak current of these analytes and the linear relations for the peak current (ip) vs. frequency (f) were observed (S.I. – 4). The linearity of the above relations suggested the involvement of adsorption in the oxidation. The adsorption was further confirmed by the linear relation of log ip versus log f (S.I. – 5). In all the cases the slope value (dlog f /dlog ip) was sufficiently greater than 0.5, which clearly confirmed that the oxidation process of these analytes was adsorption controlled (Zen et al., 2002).

To ensure the sensitivity of the PdNPs: pBG/AmSWCNTs/PG sensor toward these analytes, the concentration study was carried out at pH 7.4. The oxidation peak currents were linearly dependent on the concentrations as represented in Fig. 2. and the relations can be represented as:

$$ip\ (\mu A) = 0.1872\ [C\ 0.001 - 175\ \mu M] + 1{\cdot}1332\ (R^2 = 0.999);\ \text{For INO}$$

$$ip\ (\mu A) = 0.1715\ [C\ 0.001 - 200\ \mu M] + 2{\cdot}3195\ (R^2 = 0.998);\ \text{For HX}$$

$$ip\ (\mu A) = 0.1659\ [C\ 0.001 - 150\ \mu M] + 2{\cdot}7427\ (R^2 = 0.999);\ \text{For XT}$$

$$ip\ (\mu A) = 0.4109[C\ 0.001 - 200\ \mu M] + 4{\cdot}7192\ (R^2 = 0.998);\ \text{For UA}$$

The limit of detection (LOD) and limit of quantification (LOQ) were calculated by the relations 3σ/b and 10σ/b, respectively, where σ is the standard deviation of the blank signals and b is the observed slope of the calibration curve. The observed LOD and LOQ for these analytes were found as 0.95, 1.04, 1.07, 0.43 nM and 3.1, 3.4, 3.5, 1.4 nM for INO, HX, XT, and UA respectively. The LOD values were much lower than reported in the last few years using different modified sensors (Table 1).

3.3.2. Simultaneous analysis of INO, HX, XT, and UA

The simultaneous determination of INO, HX, XT, and UA has great importance due to co-existence of these four analytes; hence, the determination was carried out in three steps. In the first set of experiments, the SWVs were recorded by keeping the concentration of two analytes HX and UA constant as 25 μM and 15 μM, respectively, and the concentration of other two were varied from 25 μM to 150 μM (for INO) and 15 μM to 110 μM (for XT). Four distinguished and sharp oxidation peaks at potentials of 1344 mV, 1020 mV, 667 mV, and 284 mV were observed for INO, HX, XT, and UA, respectively (S.I. Fig. 6A). On increasing the concentration of both INO and XT, the peak currents of INO and XT increased without affecting the Ep and ip of other analytes HX and UA. In the second step, the SWVs were recorded by keeping the concentration of INO and XT constant (25 μM) and concentrations of HX and UA were increased from 25 μM to 150 μM and 10 μM to 70 μM, respectively. In this case, the enhancement in the peak current was observed without affecting the peak potential and peak current of INO and XT as presented in (S.I. Fig. 6B). Similar results were observed on keeping the concentration of one analyte constant with different concentrations of other three analytes; no influence was seen in the peak current and peak potential of any analyte. In the third step, the SWVs were recorded by increasing the concentration of all the four analytes from 25 μM each (for INO, HX) and 15 μM each (for XT and UA) to 150 μM each (for INO, HX), 110 μM (for XT) and 70 μM (for UA). The increment in the peak currents was observed for all four analyte with increasing concentrations without affecting the peak potential and peak current of any analyte as presented in (S.I. Fig. 6C). Thus, it is concluded from the observed results that simultaneous determination of these four analytes can be carried out effectively using PdNPs: pBG/AmSWCNTs/PG sensor. The anodic peak response and sensitivity for the individual and simultaneous determination of these analytes was found to be similar, which indicated that the presence of other analytes did not affect the simultaneous determination due to their co-existence.

3.4. Analytical utility

3.4.1. Interference study

Under optimized conditions, the interference studies were performed in the presence of ascorbic acid (AA), dopamine (DA), adenosine monophosphate (AMP), and inosine monophosphate (IMP) and the observed results are presented in Fig. 3. Fig. 3A shows a voltammograms recorded for a mixture of INO, HX, XT (35 μM each), and UA (20 μM) in the presence of increasing concentration of AA and DA upto 400 μM. The results observed from the Fig. 3A clearly demonstrate that presence of AA and DA does not interfere with the oxidation of these analytes. In another set of voltammetric studies, voltammograms were recorded for a mixture of INO (20 μM) and HX, XT, UA (35 μM each) in the presence of increasing concentration of AMP from 100 μM to 300 μM as shown in the Fig. 3B. It was observed that AMP did not cause interference in the oxidation of INO, HX, XT, and UA, whereas oxidation of IMP occurred at 1298 mV and interfered with INO. It was tolerated only up to 75 μM concentration in these studies.

3.4.2. Stability and reproducibility

The stability of the proposed method was evaluated at the 25 μM concentration of each analyte in a solution over a period of 30 days at pH 7.4. It was found that the peak currents of INO, HX, XT, and UA remained unchanged for the first 15 days with relative standard deviation (R.S.D.) as ± 1.79%, ± 2.16%, ± 1.92%, and ± 2.42%. After 15 days, a deviation in the peak current was noticed with increase in variations in R.S.D. values, therefore it is concluded that the sensor can be successfully used for the first 15 days. The intraday reproducibility of the PdNPs: pBG/AmSWCNTs/PG sensor was examined by recording at least eight replicate voltammograms at an interval of 1 h in the blank solution as well as in the mixture of INO, HX, XT, and UA (25 μM each). The R.S.D. values (n = 4) were observed as ± 0.56%, ± 1.44%, ± 0.72%, and ± 1.58% for INO, HX, XT, and UA, respectively, which indicated the good accuracy and reproducibility of prepared sensor.

3.4.3. Analysis in human urine and plasma samples

Purines can pass through the cell membrane in the human blood and enter to the blood stream. In general, purines are found in lower concentrations, but in the case of AMI, angina pectoris, and other ischemic diseases, the concentration of these analytes increases in blood plasma (Maiuolo et al., 2016). Thus, the applicability of the modified sensor was examined for the determination of INO, HX, XT, and UA in the blood plasma by standard addition method. The voltammograms were recorded and recovery studies were carried out after adding known concentration of different analytes. The recovery values were determined in the range 99.07–100.75% for INO, 99.44–101.56% for HX, 99.49–100.65% for XT, and 99.96–100.25% for UA and are summarized in Table 2.

A typical voltammogram of diluted urine sample is presented in Fig. 3C, which demonstrates the presence of all four analyte in the

Table 1
A comparison of analysis results of ATP metabolites at PdNPs: pBG/AmSWCNTs/PG sensor previously reported methods.

Sr. no.	Method/Electrode	Linear range (μM)	Detection limit	Real sample	Reference
INO					
1.	HPLC	0.93–18.6	372 nM	Yes	Farthing et al. (2007)
2.	SWNTs/PGE	10–1000	204 nM	Yes	Goyal et al. (2008)
3.	XO/screen-printed electrode	1–50	1000 nM	Yes	Carsol et al. (1997)
4.	PdNPs: pBG/AmSWCNTs/PG	0.001–175	0.95 nM	Yes	This work
HX					
1.	P6-TG/GCE	2–800	100 nM	Yes	Lan and Zhang (2015)
2.	(PyTS–NG)/GCE	8–200	231 nM	Yes	Luo et al. (2015)
3.	GCE/PLMT	0.02–0.1	7 nM	Yes	Ojani et al. (2013)
4.	PdNPs: pBG/AmSWCNTs/PG	0.001–200	1.04 nM	Yes	This work
XT					
1.	P6-TG/GCE	1–500	300 nM	Yes	Lan and Zhang (2015)
2.	(PyTS–NG)/GCE	8–800	83 nM	Yes	Luo et al. (2015)
3.	GCE/PLMT	0.02–0.1	4 nM	Yes	Ojani et al. (2013)
4.	PdNPs: pBG/AmSWCNTs/PG	0.001–150	1.07 nM	Yes	This work
UA					
1.	P6-TG/GCE	2–1600	60 nM	Yes	Lan and Zhang (2015)
2.	poly (BCP)/GCE	0.5–120	200 nM	Yes	Wang and Tong (2010)
3.	poly(PCV)/mwcntsCOOH/GCE	0.3–80	160 nM	Yes	Wang (2011)
4.	PdNPs: pBG/AmSWCNTs/PG	0.001–200	0.43 nM	Yes	This work

P6-TG: poly(6-thioguanine) film, **SWCNT**: single walled carbon nanotube, **(PyTS–NG):** 1,3,6,8-pyrene tetra sulfonic acid sodium salt functionalized nitrogendoped graphene, **XO**: Xanthine oxidase, **poly (BCP):** poly (bromocresol purple), **poly(PCV):** poly (pyrocatechol violet), **PLMT:** poly(L-methionine).

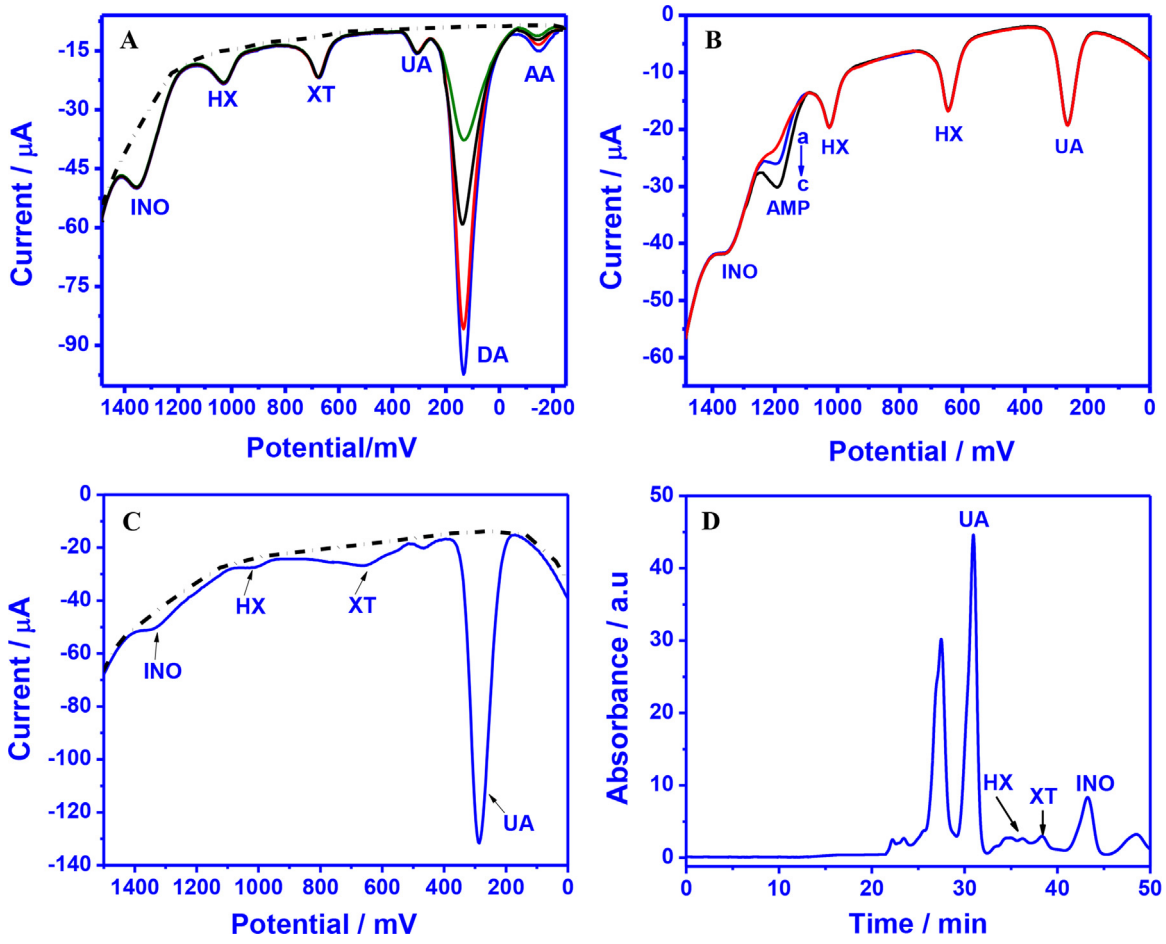

Fig. 3. (A) SWVs observed for INO, HX, XT (35 μM each), and UA (20 μM) with increased concentration of AA and DA (100 − 400 μM) for each at the PdNPs:pBG/AmSWCNTs/PG sensor at pH 7.4. The dotted line represents the background. (B) SWVs observed for INO (20 μM), HX, XT, and UA (35 μM each) in the presence of adenosine monophosphate (AMP) with increasing concentration from 100 to 300 μM; at the PdNPs:pBG/AmSWCNTs/PG sensor at pH 7.4. (C) SWV observed for human urine samples of a healthy volunteer at the modified PdNPs:pBG/AmSWCNTs/PG sensor. (D) HPLC chromatogram observed for the human urine sample of a healthy volunteer.

Table 2
Analysis of ATP metabolites in the human plasma and urine samples of healthy volunteers at the modified PdNPs: pBG/AmSWCNTs/PG sensor.

S. No.	Amount added (μM)	INO Amount detected (μM)	INO Recovery (%)	HX Amount detected (μM)	HX Recovery (%)	XT Amount detected (μM)	XT Recovery (%)	UA Amount detected (μM)	UA Recovery (%)
Plasma samples									
Sample 1									
1.	**0**	**14.24**	–	**1.40**	–	**4.60**	–	**56.15**	–
2.	5	19.32	100.56	6.42	101.42	9.63	100.65	61.14	99.98
3.	10	24.13	99.22	11.39	99.28	14.62	100.43	66.13	99.96
4.	15	29.20	99.71	16.38	98.57	19.59	99.78	77.17	100.03
Sample 2									
1.	**0**	**11.92**	–	**1.28**	–	**3.96**	–	**50.15**	–
2.	10	22.01	100.75	11.26	98.43	13.98	100.63	60.14	99.98
3.	20	31.94	100.16	21.29	100.78	23.94	99.49	70.19	100.07
4.	30	41.81	99.07	31.30	101.56	33.97	100.25	80.28	100.25
Urine sample									
Sample 1									
1.	**0**	***31.01***	–	***2.56***	–	***19.39***	–	***275.27***	–
2.	5	36.022	100.03	7.52	98.43	24.43	100.2	280.31	99.97
3.	25	55.97	99.87	27.55	99.60	44.45	100.3	300.49	100.05
4.	50	81.10	100.29	52.60	101.56	69.37	99.89	325.26	99.96

*The R.S.D. values for plasma and urine determination were less than ± 2.04 and ± 2.12, respectively for n = 3. The detected values are sum of metabolite present + added amount.

human urine sample. The concentration of the four targeted analytes was determined and reported in Table 2. The exogenous INO, HX, XT, and UA were then spiked in the urine sample and the SWVs were again recorded. The observed results are summarized in Table 2 and clearly demonstrated the acceptable range of recoveries as 99.87–100.29% for INO, 98.43–101.56% for HX, 99.89–100.3% for XT, and 99.96–100.05% for UA. The observed results in the human urine samples were also validated using HPLC studies. Four peaks were clearly observed at 30.95, 36.36, 38.40, and 43.21 min in the HPLC for UA, HX, XT, and INO, respectively as represented in Fig. 3D. Some other peaks were also observed, which were not identified in this study. All target analytes were then studied at different concentrations and the area under the peaks were plotted against concentration to get a calibration curve. The concentrations of UA, HX, XT, and INO in the urine sample were then calculated from the calibration curve and found as 275.27 μM, 2.57 μM, 19.38 μM, and 31.01 μM for UA, HX, XT, and INO, respectively. Thus, the practically similar values obtained for these four analytes by the two methods in the simultaneous determination demonstrated the sensitivity and practical applicability of the presented approach.

4. Conclusion

A fabricated novel sensitive and selective sensor based on polymer nanocomposite (PdNPs: pBG/AmSWCNTs/PG) has been efficiently used for the simultaneous detection of the four ATP metabolites, INO, HX, XT, and UA with excellent peak separation and enhanced sensitivity. At the PG surface, AmSWCNTs were effectively interlinked with the PdNPs and pBG composite film and exhibited excellent electrocatalytic activity with the larger surface area and increased electron transfer properties. The linear calibration curves were obtained for INO, HX, XT, and UA in the linear range as 0.001–175 μM, 0.001–200 μM, 0.001–150 μM, and 0.001–200 μM, respectively, with the detection limits of 0.95 nM, 1.04 nM, 1.07 nM, and 0.43 nM for INO, HX, XT, and UA, respectively. The common compounds AMP, AA, DA present in the physiological fluids have no interference in the oxidation of INO, HX, XT, and UA at the modified sensor whereas IMP was tolerated only upto 75 μM. The simultaneous determination of in the human urine and plasma samples was carried out and the observed results were validated using HPLC studies.

Acknowledgments

One of the authors (MR) is thankful to the University Grant Commission, New Delhi for the award of Senior Research Fellowship. This work was also supported by the National Research Foundation of Korea (NRF) grant funded by the Korea government (MSIP).

Appendix A. Supplementary material

Supplementary data associated with this article can be found in the online version at https://doi.org/10.1016/j.bios.2018.11.056.

References

Amorini, A.M, Petzold, A., Tavazzi, B., Eikelenboom, J., Keir, G., Belli, A., Giovannoni, G., Pietro, V.D., Polman, C., D'Urso, S., Vagnozzi, R., Uitdehaag, B., Lazzarino, G., 2009. Clin. Biochem. 42, 1001–1006.
Atta, N.F., Kady, M.F.E., 2010. Sens. Actuators B 145, 299–310.
Augusto, P., Farias, M., Castro, A.A., 2014. Anal. Chem. Insights 9, 49–55.
Bas, S.Z., Gulce, H., Yildiz, S., Gulce, A., 2011. Talanta 87, 189–196.
Buckley, S., Barsky, L., Weinbergand, K., Warburton, D., 2005. Am. J. Physiol. -Lung Cell. Mol. Physiol. 288, L569–L575.
Camba, A., Lendoiro, E., Cordeiro, C., Silva, I.M., Calvo, M.S.R., Vieira, D.N., Barus, J.I.M., 2014. Forensic Sci. Med. Pathol. 10, 627–633.
Carsol, M.A., Volpe, G., Mascini, M., 1997. Talanta 44, 2151–2159.
Chidawanyika, W., Nyokong, T., 2010. Carbon 48, 2831–2838.
Christian, G.D., Purdy, W.C., 1962. J. Electroanal. Chem. 3, 363–367.
Ciobotaru, C., Damian, C.M., Iovu, H., 2013. UPB Sci. Bull., Ser. B 75, 55–66.
Cooper, N., Khosravan, R., Erdmanna, C., Fiene, J., Lee, J.W., 2006. J. Chromatogr. B 837, 1–10.
Farthing, D.E., Farthing, C.A., Xi, L., 2015. Exp. Biol. Med. 240, 821–831.
Farthing, D.E., Sica, D., Hindle, M., Edinboro, L., Xi, L., Gehr, T.W.B., Gehr, L., Farthing, C.A., Larus, T.L., Fakhrya, I., Karnes, H.T., 2011. Luminescence 26, 65–75.
Farthing, D.E., Sica, D., Gehr, T., Wilson, B., Fakhry, I., Larus, T., Farthing, C., Karnes, H.T., 2007. J. Chromatogr. B 854, 158–164.
Goyal, R.N., Gupta, V.K., Chatterjee, S., 2008. Talanta 76, 662–668.
Goyal, R.N., Srivastava, S.K., Agarwal, R., 1985. Bull. Soc. Chim. Fr. 656–659.
Hamzah, H.H., Zain, Z.M., Musa, N.L.W., Lin, Y.C., Trimbee, E., 2013. J. Anal. Bioanal. Tech. S7, 1–6.
Hasko, G., Sitkovsky, M.V., Szabo, C., 2004. Trends Pharmacol. Sci. 25, 152–157.
Helenius, M., Jalkanen, S., Yegutkin, G.G., 2012. Biochim. Biophys. Acta 1823, 1967–1975.
Hussain, K.K., Akhtar, M.H., Kim, M.-H., Jung, D.-K., Shim, Y.-B., 2018. Biosens. Bioelectron. 109, 263–271.
Kim, D.-M., Kim, M.-Y., Reddy, S.S., Cho, J., Cho, C.-H., Jung, S., Shim, Y.-B., 2013. Anal. Chem. 85, 11643–11649.
Lan, D., Zhang, L., 2015. J. Electroanal. Chem. 757, 107–115.
Liaudet, L., Mabley, J.G., Pacher, P., Virag, L., Soriano, F.G., Marton, A., Hasko, G., Deitch, E.A., Szabo, C., 2001. Ann. Surg. 235, 568–578.
Luo, A., Lian, Q., An, Z., Li, Z., Guo, Y., Zhang, D., Xue, Z., Zhou, X., Lu, X., 2015. J. Electroanal. Chem. 756, 22–29.

Maiuolo, J., Oppedisano, F., Gratteri, S., Muscoli, C., Mollace, V., 2016. Int. J. Cardiol. 2013, 8–14.
Ojani, R., Alinezhad, A., Abedi, Z., 2013. Sens. Actuators B 188, 621–630.
Okuma, H., Watanabe, E., 2002. Biosens. Bioelectron. 17, 367–372.
Pedley, A.M., Benkovic, S.J., 2017. Trends Biochem. Sci. 42, 141–154.
Raj, M., Gupta, P., Goyal, R.N., Shim, Y.B., 2017. Sens. Actuators B 239, 993–1002.
Ramanathan, T., Fisher, F.T., Ruoff, R.S., Brinson, L.C., 2005. Chem. Mater. 17, 1290–1295.
Rastogi, P.K., Ganesan, V., Krishnamoorthi, S., 2014. Electrochim. Acta 147, 442–450.
Revin, S.B., John, S.A., 2012. Anal. Biochem. 421, 278–284.
Richter, T., Lockyear, L.L.S., Oleschuk, R.D., Bilitewski, U., Harrison, D.J., 2002. Sens. Actuators B 81, 369–376.
Shokrollahi, A., Firoozbakht, F., 2016. Beni-Seuf Univ. J. Appl. 5, 13–20.
Souza, L.F., Horn, A.P., Gelain, D.P., Jardim, F.R., Lenz, G., Bernard, E.A., 2005. Life Sci. 77, 3117–3126.
Vaisman, L., Wagner, H.D., Marom, G., 2006. Adv. Colloid Interface Sci. 128, 37–46.
Wang, W., Wang, L., Zou, L., Li, G., Ye, B., 2016. J. Electroanal. Chem. 772, 17–26.
Wang, S., Yang, F., Feng, K., Li, D., Zhao, J., Li, S., 2009. J. Sep. Sci. 32, 4069–4076.
Wang, Y., 2011. Colloid Surf. B 88, 614–621.
Wang, Y., Tong, L., 2010. Sens. Actuators B 150, 43–49.
Welihinda, A.A., Kaur, M., Greene, K., Zhai, Y., Amento, E.P., 2016. Cell. Signal 28, 552–560.
Zen, J.M., Lai, Y.Y., Yang, H.H., Kumar, A.S., 2002. Sens. Actuators B 84, 237–244.